Available online at www.sciencedirect.com
ScienceDirect
ELSEVIER
Quaternary Geochronology 1 (2006) 74–85
QUATERNARY GEOCHRONOLOGY
www.elsevier.com/locate/quageo

Research paper

Limited ice-sheet erosion and complex exposure histories derived from in situ cosmogenic ^{10}Be, ^{26}Al, and ^{14}C on Baffin Island, Arctic Canada

Gifford H. Miller[a,*], Jason P. Briner[b], Nathaniel A. Lifton[c], Robert C. Finkel[d]

[a]*INSTAAR and Department of Geological Sciences, University of Colorado, Boulder, CO 80309 0450 USA*
[b]*Department of Geology, University at Buffalo, Buffalo, NY 14260, USA*
[c]*Geosciences Department and NSF-Arizona Accelerator Mass Spectrometry Facility, University of Arizona, Tucson, AZ 85721 0077, USA*
[d]*Center for Accelerator Mass Spectrometry, Lawrence Livermore National Laboratory, Livermore, CA 94550, USA*

Received 6 February 2006; received in revised form 29 May 2006; accepted 2 June 2006

Abstract

Discordant cosmogenic nuclide exposure ages derived from ^{10}Be, ^{26}Al, and ^{14}C extracted from quartz in rocky summits along the eastern rim of the central Baffin Island plateau provide constraints on the efficiency of erosion by the Laurentide Ice Sheet (LIS) and on the timing and duration of ice-free conditions in the eastern Canadian Arctic. In situ ^{14}C records the duration of exposure during the present interglaciation; any previously acquired ^{14}C decayed below detection limits beneath thick LIS during the last glaciation. The in situ ^{14}C exposure ages for two samples adjacent to a cold-based local ice cap are significantly less than for a nearby ice-free summit, suggesting that an expanded local ice cap shielded the ice-adjacent sites for at least 800 years, longer than the duration of the Little Ice Age. Disequilibrium between ^{10}Be and ^{26}Al concentrations in the same samples can be realistically explained by brief (ca. 10 kyr) intervals of exposure during peak interglacials (MIS 11, 9, 7, 5e, and 1), separated by long (ca. 50–100 kyr) intervals of complete shielding by the LIS. The lack of glacial erosion for at least the past 400 kyr suggests that the LIS was frozen to its bed across much of Baffin Island throughout the Middle and Late Quaternary.

Keywords: Cosmogenic nuclide exposure dating; Arctic; Baffin Island; Glacial history; Interglaciation; Erosion

1. Introduction

The large-scale physiography of Baffin Island resembles a westward-tilted plane, a consequence of back-arc uplift during the rifting of Greenland from North America in the early Tertiary (Clarke and Upton, 1971). A topographic cross-section through central Baffin Island (Fig. 1) is typical for much of the northern half of the island. The land surface rises gently from the west coast to about 600 m asl, 150 km inland. Farther east, the land surface begins to be dissected, moderately at first, then more extremely in the fiord country through the height of land, where local relief is often >1500 m. In the transition between the gentle relief of western Baffin Island and the rugged fiord country of the east coast there are large areas of moderate relief where rounded summits are common between 800 and 1200 m asl. Many of the highest summits currently carry thin, cold-based ice caps (Fig. 2). The 6000 km^2 Barnes Ice Cap, a remnant of the Laurentide Ice Sheet (Hooke and Clausen, 1982), is the largest plateau ice cap, although most are less than 100 km^2 and only a few tens of meters thick. For the most part these ice caps are everywhere frozen to their beds, except where they are drained by steep, narrow valleys that carry outlet glaciers, which may be sliding.

Over the past 5 years, we have investigated the glacial history and ice-sheet dynamics in the Clyde Inlet region (Fig. 2), using cosmogenic nuclides in bedrock and large erratic boulders to define the limits and timing of Late Quaternary glaciation (Briner et al., 2003, 2005, 2006b; Davis et al., 2006). This work builds on extensive field mapping undertaken in the 1960s, when chronological control was dominantly provided by ^{14}C dates on marine

*Corresponding author.
E-mail address: gmiller@colorado.edu (G.H. Miller).

1871-1014/$ - see front matter © 2006 Elsevier Ltd. All rights reserved.
doi:10.1016/j.quageo.2006.06.011

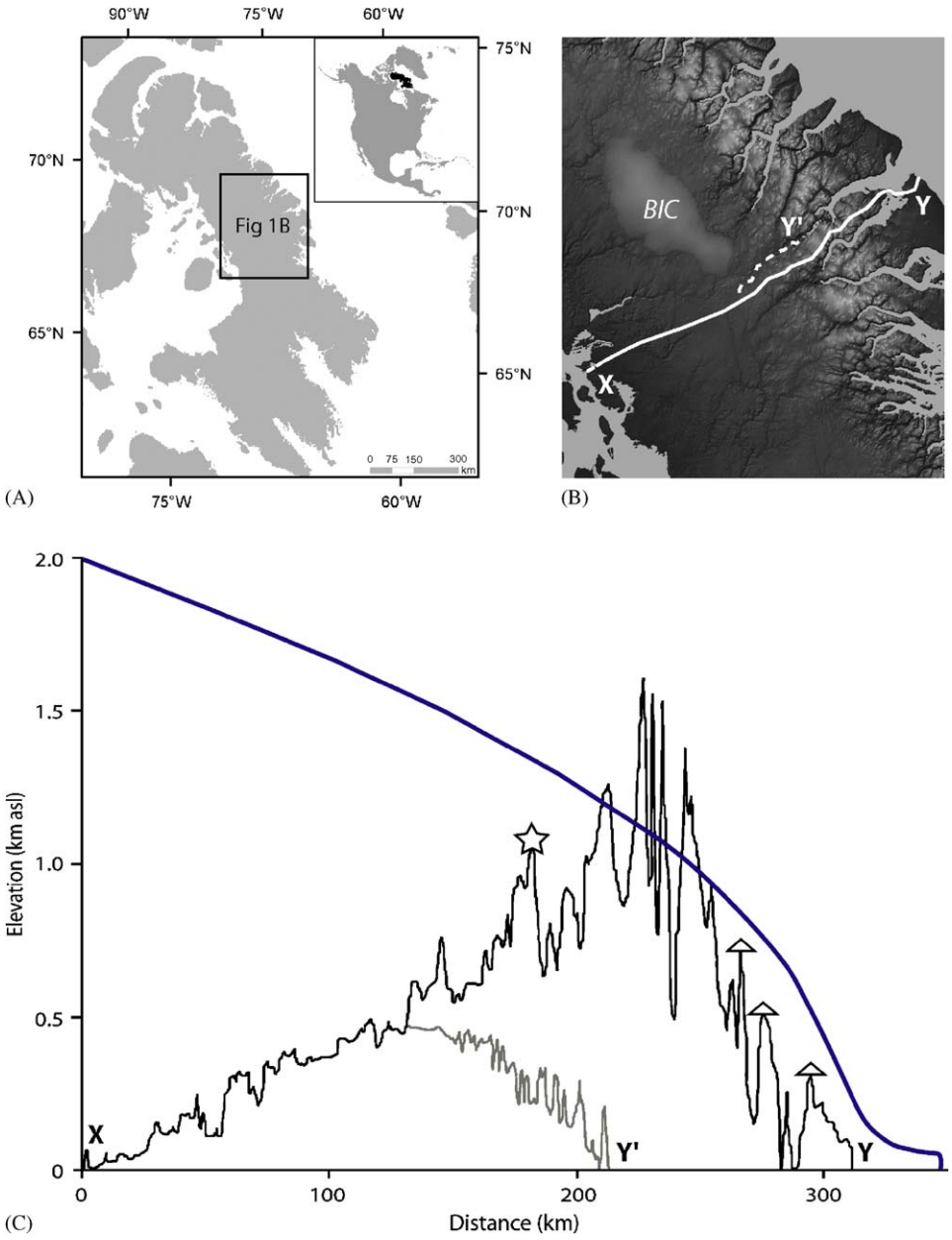

Fig. 1. Field area and regional topography. Panel A: Baffin Island, showing the location of panel B; inset shows Baffin Island (dark) in the context of North America. Panel B: Digital elevation model of central Baffin Island, showing the Barnes Ice Cap (BIC), and two cross-island profiles (panel C) that follow the height of land (*X*–*Y*; lower line) and the general thread of the Clyde River valley to the head of Clyde Inlet (*X*–*Y*′, upper line). Panel C: Topographic profiles along the lines shown in panel B. Star indicates the field site, triangles represent summits with cosmogenic-nuclide-exposure (CE)-dated Last Glacial Maximum erratics, and smooth parabolic line represents and ice-sheet profile constrained by ice physics (Kaplan et al., 1999), minimum Laurentide Ice Sheet (LIS) elevations defined by CE-dated erratics (Briner et al., 2005; Davis et al., 2006), and the minimum LIS elevation over Foxe Basin (Kaplan et al., 1999).

shells in raised marine deposits (Andrews, 1970; Andrews and Ives, 1978; Ives, 1966; Løken, 1965, 1966; Smith, 1966), and subsequent studies of the extensive section through Plio-Pleistocene sediment exposed in wave-eroded cliffs that extend for 35 km north of Clyde Inlet (Feyling-Hanssen, 1976; Miller et al., 1977).

The glacial history and ice-sheet dynamics summarized below are derived from field mapping and >250 cosmogenic nuclide exposure (CE) dates (mostly ^{10}Be) supplemented by >20 new conventional ^{14}C dates. All of the landscape west of the highest summits of Baffin Island was inundated by the Laurentide Ice Sheet (LIS) during the Last Glacial Maximum (LGM) (Briner et al., 2005, 2006b), and presumably during most earlier Middle and Late Quaternary glaciations. Outlet glaciers draining the Foxe Dome of the LIS filled most of the fiord systems of eastern Baffin Island during the LGM, terminating on the Baffin Shelf. Deglaciation of the coast occurred about 15 ka, with the fiords deglaciated about 10 ka and the fiord heads ice-free by about 8 ka. Deglaciation was accomplished both by

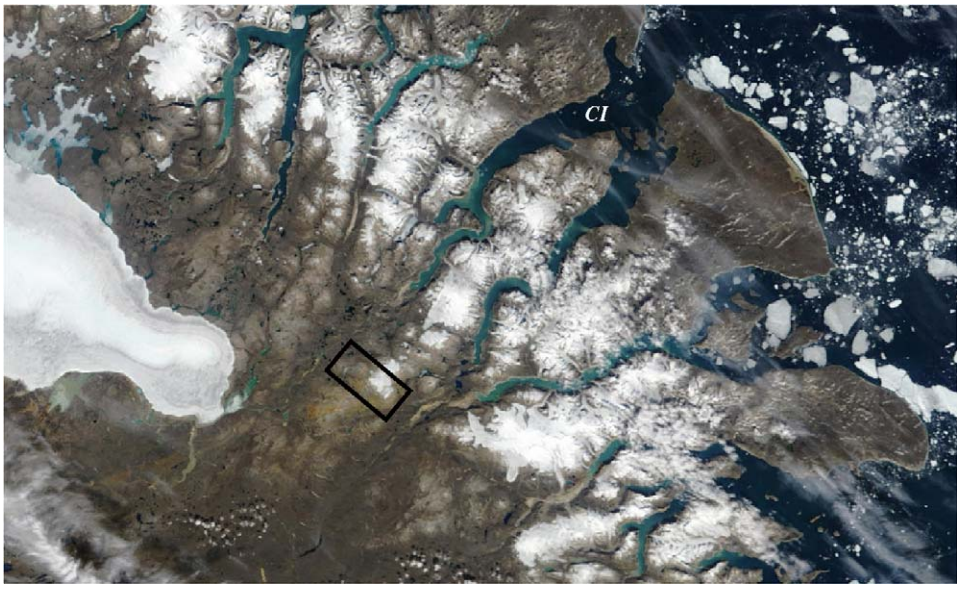

Fig. 2. Central Baffin Island, showing ice caps (white), Clyde Inlet (CI, upper right) and the location of Fig. 3 (black rectangle). Modis image from http://visibleearth.nasa.gov/.

surface lowering and marginal recession, leaving the high-elevation summits and coastal regions ice-free earliest. In contrast, valley floors, where the ice sheet was thickest, carried ice until after 6 ka, even though adjacent summits had been ice-free for several millennia (Briner et al., 2003). Based on the ^{10}Be concentrations in bedrock along vertical profiles across Clyde Inlet and nearby areas, extensive glacial erosion was limited to the primary fiord conduits, and even there, bedrock erosion sufficient to reset the cosmogenic clock occurred only in the lower 200 m or so of the fiords (Briner et al., 2006b). Away from the steep fiord confines, weathered bedrock and tor-like forms have bedrock CE ages >60 ka, but erratics resting on them have CE ages <15 ka, indicating that cold-based LGM ice invaded most of the upland regions, but performed little landscape modification (Briner et al., 2006b).

In this paper, we extend our survey into the interior, westward of the highest summits at the head of Clyde Inlet, to evaluate the potential of in situ ^{14}C to constrain the timing of deglaciation and regrowth of plateau ice caps. We combine in situ ^{14}C CE ages with CE ages from ^{10}Be and ^{26}Al measured in quartz from the same rock surfaces to address the long-term exposure history of Baffin Island during the Middle and Late Quaternary.

2. Field setting and sample sites

Clyde Inlet represents a mature fiord system, where glacial erosion has excavated the fiord head through the height of land and into the interior plateau (Fig. 1). Fast-moving, erosive ice has selectively removed rock within the fiord and valley systems, leaving the highlands mantled by less erosive, cold-based ice (Briner et al., 2006b), a process termed selective linear erosion by Sugden (1978). Our field campaign was designed to test whether differential glacial erosion continues into the interior uplands, as the physiography changes from a highly dissected fiord landscape to the rolling plateau of central Baffin Island. Samples were collected from exposed rock surfaces on local hill summits in late April 2004, when snow depths are at their maximum, minimizing the uncertainty of seasonal shielding by snow. Wind-scour limits snow accumulation on most summits, although year-to-year variability in snowfall and wind speed may result in modest snow cover in some years. However, total snowfall is low in this region (ca. 15 cm water equivalent), and most falls in spring, hence shielding by seasonal snow cover is negligible. Sample locations and elevations (± 10 m; Table 1) were determined by conventional GPS (Fig. 3). Elevation uncertainties produce a negligible uncertainty when calculating exposure ages. Sample locations are shown in Fig. 3, and the sampled surfaces are shown in Fig. 4.

Sample CR04-06 is from a summit (997 m asl) between two small, cold-based ice caps (Fig. 3). Scattered erratic blocks rest on moderately weathered bedrock with resistant vein relief of 5–8 cm, resistant knobs 10 cm across, and weathering pits up to 4 cm deep. The sample is from the surface of a quartz-rich pegmatite vein standing 6–7 cm above the host bedrock (Fig. 4a). The site is lichen-free, suggesting it was covered by ice year-round until very recently (<100 yr ago; Locke and Locke, 1977).

Samples CR04-09 and CR04-10 are from a local summit ($\sim$1160 m asl) near the current margin of a 15-km^2 ice cap (Fig. 3). Bedrock does not crop out on this summit, but large, felsenmeer slabs, which we assume are stable on Holocene time scales or longer, are common. Sample CR04-09 was collected 40 m from the current ice margin; CR04-10 was collected 150 m from the margin and 200 m from CR04-09. Sample CR04-09 was beneath the ice cap as shown in vertical aerial photography from 1961 AD, and

Table 1
Sample locations, cosmogenic nuclide measurements, and exposure ages

Sample	Lat. (N)	Long. (W)	Elevation (m asl)	Thickness (cm)	Thickness correction	[^{10}Be] (10^5 atoms g^{-1})	Site production rate (at g^{-1} yr^{-1})	^{10}Be age (ka)	[^{26}Al] (10^5 atoms g^{-1})	Site production rate (at g^{-1} yr^{-1})	^{26}Al age (ka)	^{26}Al/^{10}Be ratio	[^{14}C] (10^5 atoms g^{-1})	Site production rate (at g^{-1} yr^{-1})	^{14}C age (ka)
CR04-6	69° 34.566′	70° 44.735′	997	4	1.0331	3.9095 ± 0.1199	14.636	26.8 ± 1.6	23.232 ± 1.2235	88.2	26.6 ± 2.3	5.94 ± 0.26			
CR04-9	69° 35.674′	70° 47.202′	1157	1	1.0082	3.0635 ± 0.0966	16.818	18.2 ± 1.1	17.798 ± 0.8536	101.3	17.6 ± 1.5	5.81 ± 0.21	2.6857 ± 0.0900	45.4	10.3 ± 1.3
CR04-10	69° 35.661′	70° 47.435′	1161	4.5	1.0373	8.2609 ± 0.2509	16.876	49.5 ± 3.0	41.901 ± 1.9463	101.7	42.0 ± 3.5	5.07 ± 0.28	2.3789 ± 0.0910	45.5	8.2 ± 0.9
CR04-12	69° 37.766′	70° 52.825′	939	1	1.0082	6.1529 ± 0.1901	13.904	44.6 ± 2.7	32.378 ± 1.5038	83.8	39.3 ± 3.2	5.26 ± 0.29	2.4887 ± 0.0888	37.8	13.0 ± 2.1

Measurement uncertainties from all aspects of our extraction and analytical procedures have been fully propagated through our calculations, as have uncertainties in production rates and scaling factors. All uncertainties are reported as $\pm 1\,\sigma$. Sea level production rates are: ^{10}Be = 5.4 ± 0.1, ^{26}Al = 32.7 ± 1.5, and ^{14}C = 15.5 ± 0.2 atoms g^{-1} yr^{-1}, scaled for elevation as described in the Appendix. Rock density is 2.7 g/cm^3, and L = 160 g cm^{-2}. Measured concentrations were corrected to the rock surface using the sample thickness; no corrections were required for topographic shielding, sample geometry, or snow cover (sites are windswept and snow cover is assumed to be negligible throughout the year unless beneath an ice cap). Beryllium process blanks are $2.000 \times 10^{-14} \pm 1.287 \times 10^{-15}$ (CR04-09, -12) and $2.219 \times 10^{-14} \pm 1.199 \times 10^{-15}$ (CR04-06, -10); Al process blank is $2.733 \times 10^{-15} \pm 1.223 \times 10^{-15}$, and ^{14}C process blank is (1.4891 ± 0.1047) × 105 ^{14}C atoms. ^{14}C measurements were done at the NSF-Arizona AMS Facility; ^{10}Be and ^{26}Al were measured at CAMS, Lawrence Livermore National Laboratory.

has emerged from beneath the ice margin sometime in the past four decades, whereas CR04-10 was outside the 1961 AD ice margin. Both sites are lichen-free, indicating that CR04-10 also was beneath ice or permanent snow cover within the last century.

Sample CR04-12 is a quartz vein collected from frost-riven bedrock on a summit (939 m asl) 5 km NW of, and 220 m lower than CR04-09 and -10. The elevation difference is sufficient that this summit does not sustain a permanent ice cap, and rocks are covered with a mature, dense lichen cover. Miller (1973) showed that mature lichen cover requires more than 3 kyr to form on Baffin Island rock surfaces. Consequently, we conclude that there was no permanent snow on this summit during at least the past 3 kyr, and because this includes the portion of the Holocene when glaciers and ice caps on Baffin Island were most advanced (Miller et al., 2005), probably not since regional deglaciation.

Deglaciation of the Baffin Island plateau at the end of the LGM involved substantial lowering of the ice surface, in addition to horizontal ice retreat, as the equilibrium line was well above the top of the ice cap by 12 ka (Briner et al., 2006a). Consequently, CR04-09 and -10 must have deglaciated before CR04-12 and CR04-06, which are ca. 200 m lower. The time required for ice to thin by 200 m cannot be independently determined, but Baffin Island plateau ice caps have thinned by 0.5–1 m yr^{-1} over the past decade (Abdalati et al., 2004) and these are probably realistic estimates for thinning during the high summer insolation receipts of the early Holocene, suggesting no more than 500 yr separates the deglacial ages of these sites.

3. Methods

3.1. Scaling production rates in the polar atmosphere

Sea-level, high-geomagnetic-latitude (SLHL) production rates for ^{10}Be, ^{26}Al, and ^{14}C (Gosse and Phillips, 2001; Heisinger et al., 2002; Lifton et al., 2001; Stone, 2000) are based on mid-latitude sites where the atmosphere is significantly thicker than in the polar regions. The Appendix details how we have recalculated these values to allow for the observed sea-level pressure on Baffin Island, and for the lower sea-level atmospheric temperature and more rapid decrease in atmospheric pressure with elevation (lapse rate) in the Arctic. Combining the scaling model of Stone (2000) and our non-Standard Atmospheric model (Appendix) results in SLHL production rates for ^{10}Be, ^{26}Al and ^{14}C of 5.4 ± 0.1, 32.7 ± 1.5 and 15.5 ± 0.2 atoms g^{-1} yr^{-1}, respectively. Measurement uncertainties from all aspects of our extraction and analytical procedures have been fully propagated through our calculations, as have uncertainties in production rates and scaling factors (Bevington and Robinson, 1992). All uncertainties are reported as $\pm 1\sigma$.

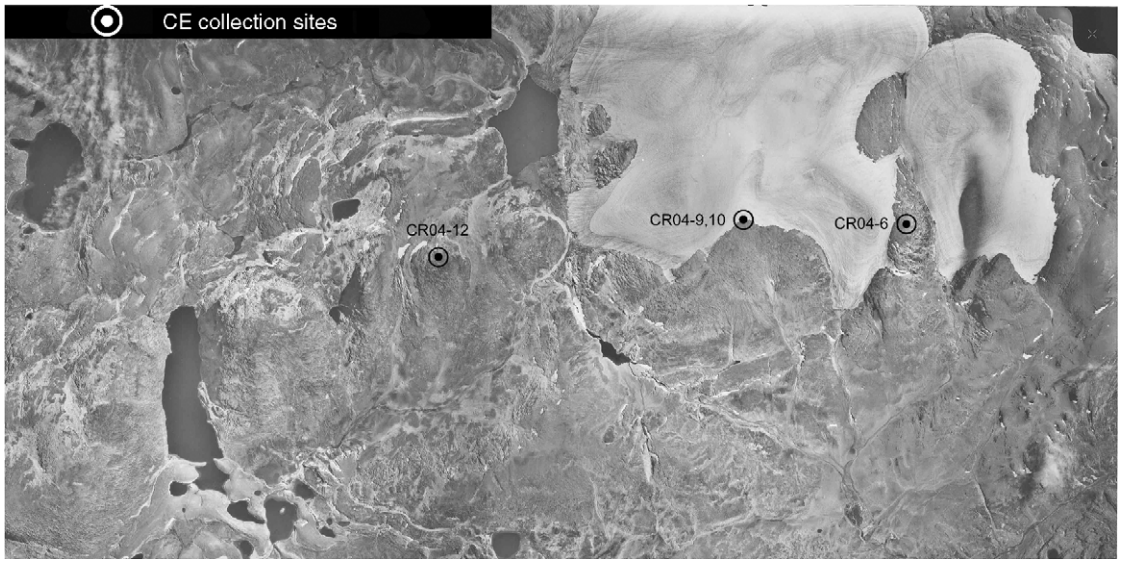

Fig. 3. Bedrock knolls from which samples were collected for cosmogenic nuclide exposure dating; Table 1 provides lat/long and elevation data. Image is a composite of vertical aerial photography by Energy, Mines, and Resources, Government of Canada.

Fig. 4. Sample collecting localities (clockwise from top left): CR04-06, CR04-09, CR04-10, and CR04-12.

3.2. *In situ* ^{10}Be *and* ^{26}Al

Samples were prepared at the University of Colorado Cosmogenic Isotope Laboratory (CUCIL) following procedures modified from Kohl and Nishiizumi (1992) and Bierman and Caffee (2001). BeO was mixed with Nb metal prior to determination of the $^{10}Be/^{9}Be$ ratios. Al_2O_3 was mixed with Ag prior to determination of the $^{26}Al/^{27}Al$

ratios by accelerator mass spectrometry at the Center for Accelerator Mass Spectrometry in the Lawrence Livermore National Laboratory $^{10}Be/^{9}Be$ isotope ratios were compared to ICN ^{10}Be standards prepared by K. Nishiizumi (pers. commun., 1995) using a ^{10}Be half-life of 1.5×10^6 yr. $^{26}Al/^{27}Al$ ratios were compared to the ^{26}Al standard prepared by Nishiizumi (2004). Site-specific production rates were corrected for topographic shielding and sample thickness using standard protocols. Because they are high-latitude sites (~70°N), cosmogenic nuclide production rates are not influenced by time-dependent changes in the geomagnetic field. We assume that for the resistant Precambrian shield rocks of Baffin Island the amount of bedrock weathering over these time intervals is negligible, an assumption supported by observations of fresh erratic boulders on the Clyde Foreland with ^{10}Be exposure ages in excess of 100 ka (Briner et al., 2005).

3.3. *In situ* ^{14}C

In situ cosmogenic ^{14}C was extracted from quartz separates of samples CR04-09, CR04-10, and CR04-12 using methods modified from Lifton et al. (2001) and Pigati (2004). The extraction process involves combusting ~5 g of quartz at 500 °C for 1 h to remove atmospheric contaminants, followed by dissolution in a degassed $LiBO_2$ flux at 1100 °C for 3 h. Both steps take place in an atmosphere of 50 torr of ultra-high-purity O_2. Any carbon species released during the high-temperature step are oxidized to CO_2, which is then purified, measured quantitatively, and converted to graphite for ^{14}C measurement by accelerator mass spectrometry (Lifton et al., 2001). The extraction procedures described by Pigati (2004) achieve an ~30% reduction in the time necessary to complete the extraction process relative to those detailed in Lifton et al. (2001). Blank values for the shorter extraction procedure are correspondingly lower as well (Table 2). Pigati (2004) utilized a simpler extraction system than that used by Lifton et al. (2001), but with the shorter procedures, both systems yield indistinguishable results at the 1σ level for the wave-cut quartzite bedrock shoreline associated with the Lake Bonneville highstand (Promontory Point, Utah; sample PP-4) analyzed by Lifton et al. (2001). However, the weighted mean of the in situ ^{14}C concentrations extracted from PP-4 using the new procedures is approximately 7% lower than the value measured by Lifton et al. (2001) (Table 2). We believe this reflects the fact that the simpler extraction procedures present fewer opportunities for inadvertently introducing small amounts of contaminant ^{14}C into the sample.

These new measurements yield a revised in situ ^{14}C production rate at the Lake Bonneville calibration site (41.264°N, −112.480°E, 1594 m altitude) of 49.2 ± 0.7 atoms g^{-1} yr^{-1}, integrated over the last 17.4 ± 0.3 cal kyr (Lifton et al., 2001). We assumed the proportion of in situ ^{14}C production by high-energy nucleon spallation to that by both fast and slow muons at SLHL was 0.83:0.17 (Table 3; Heisinger et al., 2002).

Table 2
New analyses of sample PP-4 from the wave-cut quartzite bedrock shoreline associated with the Lake Bonneville high stand at Promontory Point, Utah

Lab ID	AMS ID[a]	Sample mass[b] (*g*)	In situ ^{14}C concentration[c] ($\times 10^5$ at g^{-1})
RN-661	AA61595	5.0073	3.4359 ± 0.1626
RN-662	AA61596	5.0062	3.4996 ± 0.1640
RN-665	AA61597	4.9971	3.4939 ± 0.2122
RN-674	AA34075	5.0042	3.5950 ± 0.1591
RN-687	AA61597	4.9983	3.8008 ± 0.1665
RN-690	AA34075	4.9972	3.6889 ± 0.1612
RN-691	AA34075	5.0075	3.5365 ± 0.1522
RN-704	AA61597	5.0030	3.3816 ± 0.1441
RN-748	AA34075	5.0071	3.6799 ± 0.1570
RN-758	AA61597	4.9978	3.5184 ± 0.1522
Weighted mean			3.5687 ± 0.0510

All uncertainties are $\pm 1\sigma$

[a] AA34075 analyses used the original extraction system of Lifton et al. (2001), but with new procedures. The new weighted mean blank value for this system is $(1.4891 \pm 0.1047) \times 10^5$ ^{14}C atoms ($n = 8$). AA61597 analyses used the simplified extraction system of Pigati (2004). The weighted mean blank value for this system is $(2.3998 \pm 0.1215) \times 10^5$ ^{14}C atoms ($n = 10$).

[b] Uncertainty = ±0.0002 g.

[c] Normalized to the ground surface (correction factor 1.0779 ± 0.0106), no topographic shielding (correction factor 1.0064 ± 0.0255) and SiO_2 composition (correction factor 1.0027 ± 0.0266).

3.4. *Ice-sheet shielding*

The thickness of ice required to completely inhibit production of cosmogenic nuclides in a rock surface beneath the ice can be calculated theoretically. For ^{14}C, a realistic detection limit is about five times the blank uncertainty of ~11,000 atoms. Using established ^{14}C production proportions, appropriate attenuation lengths, and an ice density of 0.917 g cm^{-3} (Table 3), predicted in situ ^{14}C concentrations remain at or below the ^{14}C detection limit under ⩾35 m of ice at 1000 m asl and 70°N latitude, regardless of burial duration. Although muon production amounts to a significantly smaller fraction of the total ^{10}Be and ^{26}Al produced cosmogenically (Table 3), the long half-lives of these nuclides and high proportion of time beneath ice for these samples, require even thicker ice (⩾100 m) to reduce muon-produced nuclides to background levels.

The actual ice thickness over the collection sites during the LGM can be estimated using ice-sheet profiles constrained by the terminal position of the LIS, the elevations of CE-dated LGM erratics, and ice-sheet modeling that defines a minimum ice thickness over Foxe Basin. CE-dating along Clyde Inlet, directly down-ice from our field sites, confirms that outlet glaciers of the LIS terminated on the Baffin Shelf during the last glaciation, and only receded back to the present coastline ca. 15 ka (Briner et al., 2005; Davis et al., 2006). This provides an approximate ice-margin at the LGM (Fig. 1). The highest

Table 3
Proportions of cosmogenic nuclide production due to various mechanisms (from Heisinger et al., 2002)

Production mechanism	^{14}C (%)	^{10}Be (%)	^{26}Al (%)	Attenuation length (g cm^{-2})
Spallation	83	96.39 ± 0.36	95.44 ± 0.48	160
Fast muon	2	1.69 ± 0.24	2.15 ± .026	4300
Slow muon	15	1.92 ± 0.13	2.42 ± 0.22	1500

CE-dated LGM erratics along this profile (Fig. 1) place a minimum elevation for the ice-sheet profile along Clyde Inlet. The ice-sheet modeling of Kaplan et al. (1999) concluded that in Foxe Basin, at the west end of our profile, the LIS must have been at least 2 km thick. Most other modeling efforts (e.g. Hughes, 1998) suggest even thicker ice. A realistic ice-sheet profile that meets these constraints (Fig. 1) indicates the ice surface was ~1400 m asl at our field area, >200 m above our highest site, and therefore sufficiently thick during the LGM to attenuate all radionuclide production in the underlying surfaces.

4. Results

Three samples (CR04-09, CR04-10, and CR04-12) have apparent exposure ages derived from the measured concentrations of all three cosmogenic nuclides, ^{10}Be, ^{26}Al, and ^{14}C; both ^{10}Be, ^{26}Al concentrations were measured in CR06-06, the fourth sample (Table 1).

Sample CR04-12, collected from the summit currently lacking an ice cap, has discordant exposure ages from all three cosmogenic nuclides. In situ ^{14}C, with the shortest half-life, yields the youngest age (13.0 ± 2.1 ka) for this sample, whereas ^{10}Be, with longest half-life, yields the oldest age (44.6 ± 2.7 ka), with the ^{26}Al age slightly younger (39.3 ± 3.2 ka). The ^{26}Al/^{10}Be ratio (5.26 ± 0.29) is significantly below the equilibrium ratio of ~6.0 for continuously exposed samples. These data are consistent with a long and complex exposure history dominated by burial (Lal, 1991; Bierman et al., 1999; Phillips et al., 2006).

Sample CR04-09 emerged from beneath the adjacent ice cap after 1960 AD. Because the site is on a drainage divide, there is little chance that meltwater flowing along the melting ice margin would have removed overburden, and we consider the rock to have been continuously at the ground surface at least since regional deglaciation. CR04-09 also yields an in situ ^{14}C concentration that provides the youngest CE age (10.3 ± 1.3 ka) for this sample, although in this case the ^{10}Be and ^{26}Al ages are older, but statistically indistinguishable (18.2 ± 1.1 and 17.6 ± 1.5 ka, respectively). The ^{26}Al/^{10}Be ratio (5.81 ± 0.21) is not significantly different from a continuous exposure value of ~6.0.

Sample CR04-10 is only 200 m from CR04-09 and in a similar setting. It has the youngest in situ ^{14}C age (8.2 ± 0.9 ka), but the highest concentrations of ^{10}Be and ^{26}Al nuclides of the four samples. The apparent exposure age derived from its ^{10}Be inventory is 49.5 ± 3.0 ka, significantly older than the apparent exposure age derived from the ^{26}Al inventory of 42.0 ± 3.5 ka. This difference translates to an ^{26}Al/^{10}Be ratio of 5.07 ± 0.28, well below the predicted value of ~6.0 for a continuously exposed sample.

Because samples CR04-09 and -10 are from nearly the same locality, we average the [^{14}C] of the two samples to reduce random errors in the measurement of in situ ^{14}C. Weighting by the reciprocal of the squared relative uncertainty in each measurement and using weighted average variance (Bevington and Robinson, 1992), we derive a weighted mean [^{14}C] = 2.5521 ± 0.1517 × 10^5 atoms g^{-1}, and 9.1 ± 1.0 kyr for the weighted mean exposure age (in both cases, the weighted average variance was larger than the uncertainty in the weighted mean, so we used the former value to be conservative). Although the difference in measured [^{14}C] in these two samples is relatively large, our sample size is small, and the weighted average variance on the mean is our best estimate of how well we know the mean value (corresponding to the standard error for an unweighted mean).

CR04-06 was collected from a summit that was ice-covered within the past century. The concentrations of ^{10}Be and ^{26}Al produce statistically indistinguishable apparent exposure ages of 26.8 ± 1.6 and 26.6 ± 2.3 ka. These ages demand a longer exposure history than possible in the postglacial interval but the ^{26}Al/^{10}Be ratio (5.94 ± 0.26) does not require a long, complex burial history.

5. Interpretation

Ice cover in excess of 100 m will attenuate cosmic rays so that no significant production of any of the nuclides we measured would occur in rock beneath the ice. Ice thicknesses between 35 and 100 m will allow some muogenic production of ^{10}Be and ^{26}Al, but muogenic production rates are low, so the ice must remain at this thickness for long intervals to allow significant nuclide accumulation in underlying rocks. For ice thicknesses <35 m, nuclide production increases rapidly with thinning ice. The ice-sheet profile fit to field evidence (Fig. 1) suggests the ice surface was 200–400 m above the collection sites during the LGM, sufficient to attenuate all nuclide production. It is not possible to reconstruct ice thickness over the collection sites through the Middle and Late Quaternary, but our evidence from the coastal regions indicates the LIS was most extensive, hence thickest, early

in the last glacial cycle. Consequently, we model the exposure history at our collection sites as either covered by thick ice with no production of cosmogenic nuclides, or exposed to the full cosmic ray flux.

5.1. *In situ ^{14}C exposure ages*

The lack of any unambiguously finite radiocarbon ages on marine shells between about 12 and 40 cal ka from anywhere on Baffin Island (Dyke et al., 2001) suggests that the NE sector of the LIS was near its maximum configuration from at least 40 ka until nearly 12 ka, although recent ^{10}Be CE dates suggest deglaciation of the coastal reaches began by 15 ka (Briner et al., 2005, 2006b). By 10 ka, most of Clyde Inlet was ice free (Briner et al., 2006b), by which time the high-elevation summits near the fiord heads should have been ice-free. Summits may have been exposed a few millennia before the fiords if vertical lowering under the high summer insolation of the early Holocene was the dominant ablation process. This interpretation is supported by the pattern of deglacial moraines showing that the latest ice lay in the deepest valleys, and the CE ages of LGM erratics that are oldest on the highest summits, and decrease in age at lower summit elevations (Briner et al., 2003, 2005, 2006b). Shielding by $\geqslant$100 m of LIS for $\geqslant$25 kyr is sufficient for all previously acquired in situ ^{14}C to have decayed below our detection level (Fig. 5). Within the uncertainties, the in situ ^{14}C exposure age of 13.0 $\pm$ 2.1 ka (CR04-12) is consistent with continuous shielding beginning prior to 40 ka until deglaciation, followed by continuous exposure. The younger in situ ^{14}C exposure ages for the ice-cap-proximal samples CR04-09 and -10, are consistent with continuous shielding since at least 40 ka, but suggest a more complex Holocene exposure history (see below). On the other hand, the relatively high concentrations of ^{10}Be and ^{26}Al in all four samples (Table 1) require significant pre-LGM exposure of the rock surfaces.

The in situ ^{14}C exposure age for CR04-12 (939 m asl) is significantly greater than for either CR04-09 (1157 m asl) or CR04-10 (1161 m asl), despite the lower elevation, hence later LIS deglaciation of CR04-12. This enigma can be explained either by post-deglaciation disturbance for samples -09 and -10 or post-deglaciation shielding of these sites that did not occur at site -12. The high ^{10}Be and ^{26}Al CE ages at sites -09 and -10 (Table 1) argue against significant disturbance, whereas their position at the margin of a thick local ice cap offers the potential of shielding by its late Holocene expansion. In contrast, mature lichen cover at CF04-12 indicates it has been continuously exposed since deglaciation.

The burial history for sites -09 and -10 can be modeled with minimal assumptions. We use the average exposure age of 9.1 $\pm$ 1 ka and average [^{14}C] of 2.5521 $\pm$ 0.1517 $\times$ 10^5 atoms, and assume that the LIS uncovered all three sites ca. 13 ka and that regrowth of local mountain ice caps occurred in the late Holocene, consistent with glacial records elsewhere on Baffin Island (Miller et al., 2005). There are, of course, an infinite number of exposure histories that could fit the observed differences in [^{14}C]. We model only the simplest option, a single latest Holocene local ice-cap expansion, shielding sites CR04-09 and -10 for a sufficient duration to reduce their [^{14}C] inventories to the observed levels. This scenario requires that the ice cap covered the two sites 1000 $\pm$ 200 years ago, and only melted back to expose them again in recent decades (Fig. 5).

The duration of recent ice cover over CR04-09 and -10 required to explain the differences in their ^{14}C inventories from that at CR04-12 is relatively insensitive to uncertainties in production rate or deglaciation date. If deglaciation at both sites occurred 12 ka, rather than 13 ka, the duration of recent ice cover is reduced to 800 $\pm$ 200 years (fine red line, Fig. 5); alternatively if the sites were deglaciated 14 ka, then the duration of burial increases to 1200 yr. If the lower site (CF04-12) deglaciated significantly later than sites -09 and -10, the duration of late Holocene ice shielding at -09 and -10 necessarily would be greater. Alternatively, if the production rates we use are too low, and the actual date of deglaciation is, for example, 10 ka rather than 13 ka at both sites, the duration of CR04-09 burial is 1000 yr, the same as in our initial scenario. Based on these assessments of uncertainty, our calculated estimate of 1000 $\pm$ 200 yr late Holocene ice cover at -09 and -10 is most probably a minimum estimate.

5.2. *Long-term burial history from ^{10}Be and ^{26}Al concentrations*

The relatively high concentrations of ^{10}Be and relatively low ^{26}Al/^{10}Be ratios in samples CR04-10 and -12 can only be explained if the cumulative burial history greatly exceeds the duration of cumulative exposure. The proportion of time these sites were shielded can be modeled following Lal (1991), assuming no loss of rock due to erosion. The preservation of rock surfaces beneath cold-based ice, and modeling complex ice-cover histories based on disequilibrium between cosmogenic isotope pairs has been reported by Kleman and Stroeven (1997), Bierman et al. (1999), Stroeven et al. (2002), and Fabel et al. (2006).

Because a wide range of exposure and burial histories can explain the ^{10}Be and ^{26}Al inventories, we set out a realistic working hypothesis to be tested by the model. We hypothesize that upland summits on the interior plateau of Baffin Island are only free of thick LIS or local ice-cap cover during peak interglaciations, typically of no more than 10 kyr duration. During the intervening "glacial" periods, the sites lay beneath sufficient ice to attenuate the flux of cosmic particles.

To model the scenario described above, we utilize long records from the Antarctic Ice Sheet (EPICA Community Members, 2004) and deep-sea δ^{18}O of benthic organisms (Imbrie et al., 1993) that carry a global climate signal. We use the odd-numbered marine isotope stage (MIS) designations of interglacials. Ice core and marine records show

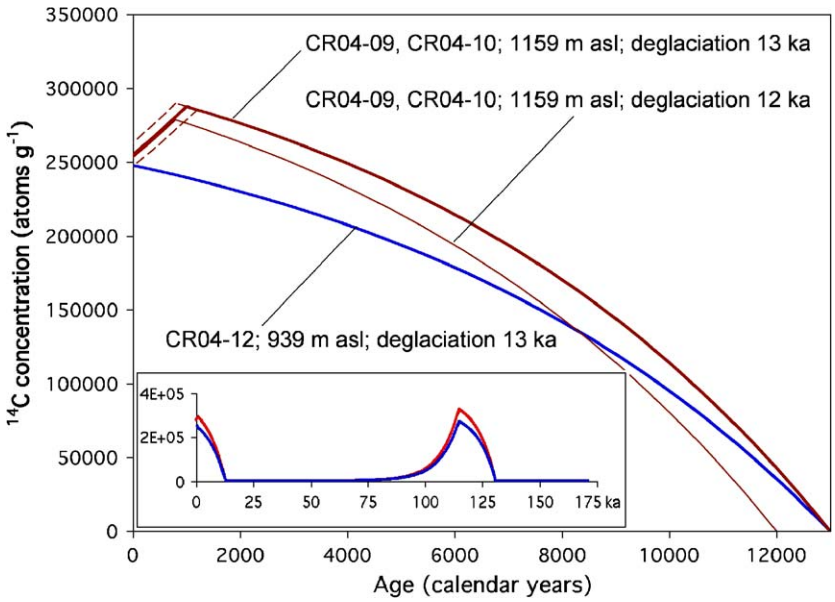

Fig. 5. Modeled in situ ^{14}C inventories in samples CR04-09/10 and CR04-12. Thick solid lines assume that both sites were deglaciated 13 ka with no inheritance and that CR04-09 became ice-cap-covered 1000 years ago. Dashed lines show the evolution using 1 sigma uncertainties on the [^{14}C] of CR04-09/10. Thin line shows the evolution of [^{14}C] for CR04-09/10 if deglaciation at both sites had occurred 12 ka instead of 13 ka. Inset (lower left) shows the ^{14}C inventories over the past 175 kyr, following the prescribed exposure history used for Fig. 6 (upper line is CR04-09.10, and lower line is CR04-12, which has a lower production rate because it is at a lower elevation).

peak warmth during MIS 5e, a relatively weak warming in MIS 7, peak warmth again in MIS 9 and a relatively long warm peak in MIS 11. We allocate 10 kyr of ice-free conditions at our sites during MIS 5e and 9, but only 6 kyr for the weaker MIS 7. MIS 11 is recognized as a long interglacial in both Antarctic and marine cores; consequently, we allow 17 kyr of exposure during MIS 11. Marine and ice-core records indicate that earlier Middle Quaternary interglaciations lacked the warmth of MIS 11 and later. The ^{10}Be and ^{26}Al inventories indicate that our oldest sites were eroded (that is, the exposure clock was last reset) prior to MIS 11. During all intervening times after MIS 11 not specifically identified as ice-free above (ca. 360 kyr of cumulative time) our sites are designated as covered by >100 m of ice, effectively eliminating the production of cosmogenic nuclides.

The evolution of [^{10}Be] and ^{26}Al/^{10}Be for the two oldest samples using the scenario outlined above (Fig. 6, upper panel) produces [^{10}Be] consistent with what was measured in these samples, and ^{26}Al/^{10}Be ratios within the uncertainties of the measured ratios. Following the same guidelines for the two younger samples (Fig. 6, lower panel) yields the appropriate [^{10}Be] for both samples (with two interglacial exposures for CR04-09, and three interglacial exposures for CR04-06), while also reaching ^{26}Al/^{10}Be within the uncertainties of the measurements.

Although there is no evidence that the LIS slid at these sites (no glacial abrasion), the relatively young exposure ages for CR04-06 and CR04-09 compared to the other two samples requires some geomorphic work to occur in the Middle Quaternary. We speculate that ice frozen to its bed occasionally moved blocks or sheared off bedrock that protruded into the ice and was vulnerable to differential flow in the lowest layers of the ice sheet (Cuffey et al., 2001; Atkins et al., 2002), a conclusion similar to that of Phillips et al. (2006) for the Scottish Highlands. In our two-felsenmeer samples, the lower [^{10}Be] and [^{26}Al] in CR04-09 relative to CR04-10, only 200 m distant, might be explained by a MIS 6 disturbance of CR04-09. However, because none of our sites had ^{10}Be concentrations consistent with exposure only in the Holocene, it is unlikely that any significant erosion was achieved at these sites since the last interglaciation.

6. Conclusions

The concentrations of the in situ cosmogenic nuclides ^{14}C, ^{10}Be, and ^{26}Al in rocks from local hill summits that have remained within the cold-based (non-erosive) zone of the LIS provide significant constraints on ice-sheet history.

- In situ ^{14}C provides a reliable measure of the postglacial exposure history for stable rock surfaces that were buried for >25 kyr beneath a thick (>35 m) ice-sheet cover.
- Differences in in situ ^{14}C concentrations for two sites deglaciated at about the same time can be explained by ca. 1000 yr of late Holocene burial beneath an expanded local ice cap. This duration is longer than the Little Ice Age, suggesting a complex history of Neoglacial growth and decay for the thin, cold-based ice caps of the Baffin Island plateau.

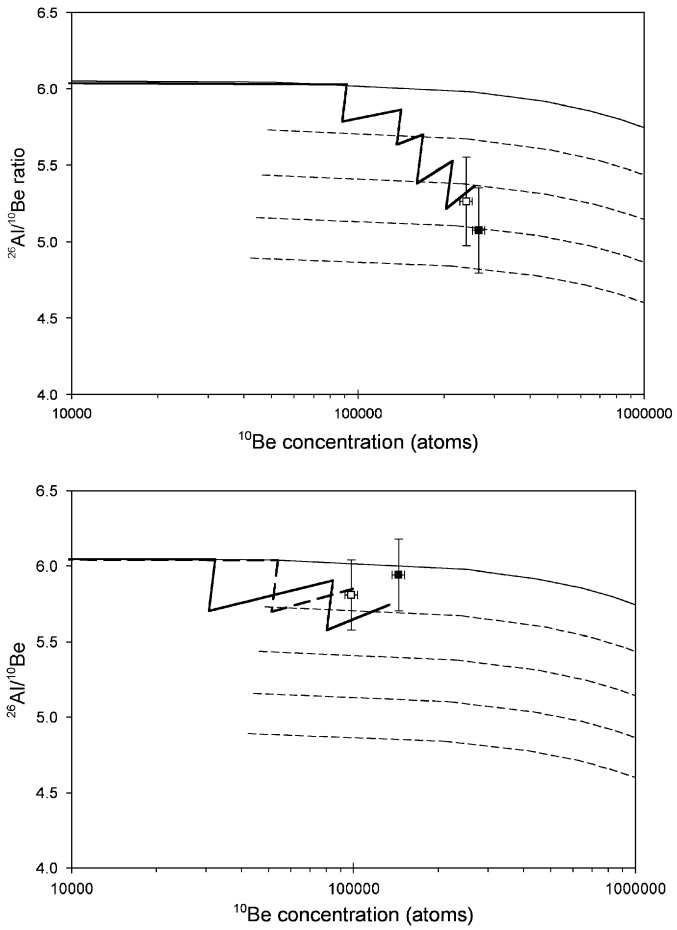

Fig. 6. Modeled exposure histories for the four samples discussed in the text, based on their [^{10}Be] and ^{26}Al/^{10}Be, assuming exposure only during peak interglaciations, and no cosmogenic nuclide generation during intervening glaciations. Thin, solid line is the trajectory for samples with no burial, dashed lines indicate burial of 100, 200, 300, and 400 kyr, respectively, following a single exposure history. Upper panel Samples CR04-10 (solid square) and CR04-12 (open square) were both exposed during MIS 11 (17 kyr), MIS 9 (10 kyr), MIS 7 (6 kyr), MIS 5e (10 kyr) and MIS 1 (10 kyr). The cosmogenic clock was last reset prior to MIS 11 for both samples. Lower panel Exposure histories for samples CR04-06 (solid line; solid square) and CR04-09 (dashed line; open square). CR04-06 received exposure during MIS 7 (6 kyr), 5e (10 kyr) and MIS 1 (10 kyr), whereas CR04-09 (dashed line) was first exposed in MIS 5e (10 kyr) and again in MIS 1 (9 kyr exposure followed by 1 kyr burial). These results suggest that CR04-09 (felsenmeer) may have been reset during MIS 6, and CR04-06 (bedrock) in MIS 8, whereas the other two samples have been undisturbed since before MIS 11.

- The concentrations of ^{10}Be and ^{26}Al found in all four summit samples can be explained by brief (~10 kyr) intervals of exposure during peak warmth of Quaternary interglaciations, separated by relatively long (50–100 kyr) intervals during which the sites were covered by >100 m of ice, shielding them from cosmogenic nuclide production. To meet this condition, the northern sector of the LIS must have grown early in each glacial cycle and remained intact until the next interglaciation. Local ice cap growth late in the interglaciations, as demonstrated by the ^{14}C data, may shield some sites more than others.
- The lack of glacial erosion over the past 400 kyr on summits only 500–800 m above striated valley floors, suggests that the NE sector of the LIS was wet-based only in restricted areas where it fed outlet glaciers in the fiord systems, and that over much of Baffin Island, the ice sheet was frozen to its bed throughout this time interval.

Acknowledgements

Field work on Baffin Island was supported by NSF Grant OPP- 0138586; we thank the Inuit of Clyde River for access to the field area and helpful advice and assistance with the field campaign. Extraction and analysis of in situ ^{14}C was supported by NSF Grant ARC-0454662, with assistance from the NSF-Arizona AMS Facility. ^{10}Be and ^{26}Al measurements were performed under the auspices of the US Department of Energy by the University of California, Lawrence Livermore National Laboratory under Contract no. W-7405-Eng-48, and with the support of NSF Grant OPP- 0138586. We thank Rebecca Anderson and Jackson Crews for assistance with sample processing, and Stephen DeVogel for assistance with figures. Reviews by Ted Little (GSC), John Gosse (Memorial University) and an un-named referee helped to clarify many of the points in the manuscript, and are greatly appreciated.

Appendix: Scaling production rates in the polar atmosphere

Probably the most commonly cited sea-level, high-geomagnetic-latitude (SLHL) production rates for ^{10}Be and ^{26}Al are 5.1 and 31.1 atoms g^{-1} yr^{-1}, respectively (Stone, 2000; Gosse and Phillips, 2001). Because SLHL production rates are typically scaled from non-SLHL locations, their values are inherently tied to the assumptions used in the scaling procedure. These values were derived assuming the Standard Atmospheric model (National Oceanic and Atmospheric Administration, 1976), which approximates average mid-latitude atmospheric conditions. However, Stone (2000) also demonstrated that spatial variations in long-term mean sea-level pressure can affect cosmogenic nuclide production rates significantly. Similar spatial variations in mean sea-level temperature and lapse rate can also affect how production rates scale with altitude and latitude (e.g., Dunai, 2000). These departures from the spatially invariant Standard Atmosphere are generally greatest near the poles and in the tropics—we thus required a spatially variable atmospheric model to account for this in our study area. It is essential that production rate scaling uses an internally consistent framework. Changing the scaling assumptions requires corresponding recalculation of the SLHL production rates. To do this, one needs to start with the original calibration site production rate measurements for each nuclide.

We recalculated the ^{10}Be production rate using 6 calibration sites for which primary ^{10}Be concentrations were readily available or easily derived. Bierman et al. (1996) give the mean value of 12 analyses from a Laurentide terminal moraine in New Jersey. Gosse and Klein (1996) provide a measurement from a wave-cut bedrock shoreline from Pleistocene Lake Bonneville in Utah, similar to that used by Lifton et al. (2001), and a measurement from the Titcomb Basin Moraine in the Wind River Range of Wyoming. We limited our use of measurements from Nishiizumi et al. (1989) to two near-horizontal samples (W86-3 and W86-10), since they did not require additional significant sample slope corrections. Finally, we used the mean concentration of 8 samples from the Koeffels landslide in Austria: KOE4, KOE5, KOE6, KOE20, KOE101 (Kubik and Ivy-Ochs, 2004; Kubik et al., 1998) and BK1, BK4, BK5 (Abramowski, 2004). For the ^{26}Al production rate recalculation, we used measurements from 4 calibration sites: the two near-horizontal samples from Nishiizumi et al. (1989), the weighted mean of three Koeffels measurements (KOE4, KOE5, KOE6; Kubik et al., 1998), and the mean of 14 measurements from the Laurentide sites given in Bierman et al. (1996). The new ^{14}C calibration site data are presented in Table 2 and discussed in the main text.

We used the scaling formulations of Stone (2000) to scale the calibration site production rates to SLHL for the ^{10}Be, ^{26}Al and ^{14}C calculations, and to our sampling locations, although several other scaling models have been proposed (Desilets and Zreda, 2003; Dunai, 2000, 2001; Lifton et al., 2005). We use the production proportions for high-energy nucleon spallation and for total muons (fast + slow) given for each nuclide by Heisinger et al. (2002, Table 3). Site atmospheric pressures were calculated using the Standard Atmosphere equation (National Oceanic and Atmospheric Administration, 1976, Eq. (33a)), substituting mean annual sea-level pressures, model sea-level temperatures and generalized model lapse rates for the corresponding standard values. Sea-level pressures were interpolated from a 2.5° latitude–longitude grid derived from the 1979–1998 monthly mean NCEP/NCAR Global Reanalysis dataset (http://dss.ucar.edu/datasets/ds090.0/data/cdrom/monthly/data/clim/c7998/prmsl.grb). Mean annual sea-level temperatures were derived from a latitudinal fit to the CIRA-86 atmospheric model (http://nssdc.gsfc.nasa.gov/space/model/atmos/cospar2.html) (Lifton et al., 2005, Appendix A.1). Generalized lapse rates were estimated with the following fit to the CIRA-86 model atmosphere below 10 km altitude ($r^2 = 0.994$):

$$\text{L.R.} = a + b\lambda + c\lambda^2 + d\lambda^3 + e\lambda^4 + f\lambda^5 + g\lambda^6, \qquad \text{(A1)}$$

where λ is latitude ($-80 < \lambda < 80$), $a = -6.15 \times 10^{-3}$, $b = -3.18 \times 10^{-6}$, $c = -1.50 \times 10^{-7}$, $d = 1.81 \times 10^{-9}$, $e = 1.18 \times 10^{-10}$, $f = -6.54 \times 10^{-14}$, and $g = -9.52 \times 10^{-15}$.

Predicted SLHL production rates were then calculated for ^{10}Be, ^{26}Al, and ^{14}C; weighted means were calculated for the ^{10}Be and ^{26}Al values. The resulting SLHL production rates account for departures from the Standard Atmosphere both at the calibration sites and at SLHL locations, and are appropriate for our assumed variable atmospheric model. The recalculated rates are 5.4 ± 0.1 atoms g^{-1} yr^{-1} for ^{10}Be, 32.7 ± 1.5 atoms g^{-1} yr^{-1} for ^{26}Al, and 15.5 ± 0.2 atoms g^{-1} yr^{-1} for ^{14}C.

References

Abdalati, W., Krabill, W., Frederick, E., Manizade, S., Martin, C., Sonntag, J., Swift, R., Thomas, R., Yungel, J., R., K., 2004. Elevation changes of ice caps in the Canadian Arctic Archipelago, J. Geophys. Res., 109:doi:10.1029/2003JF000045.

Abramowski, U., 2004. The use of ^{10}Be surface exposure dating of erratic boulders in the reconstruction of the late Pleistocene glaciation history of mountainous regions, with examples from Nepal and Central Asia. Ph.D. Thesis, University of Bayreuth, 167 pp.

Andrews, J.T., 1970. A geomorphological study of post-glacial uplift with particular reference to Arctic Canada, special publication number 2. Institute of British Geographers.

Andrews, J.T., Ives, J.D., 1978. "Cockburn" nomenclature and the late Quaternary history of the eastern Canadian Arctic. Arctic Alpine Research 10, 617–633.

Atkins, C.B., Barrett, P.J., Hicock, S.R., 2002. Cold glacies erode and deposit: evidence from Alan Hills, Antarctica. Geology 30, 659–662.

Bevington, P.R., Robinson, D.K., 1992. Data Reduction and Error Analysis for the Physical Sciences. McGraw-Hill, New York, 328 pp.

Bierman, P.R., Caffee, M., 2001. Steady state rates of rock surface erosion and sediment production across the hyperarid Namib Desert and the Namibian escarpment, southern Africa. American Journal of Science 301, 326–358.

Bierman, P., Larsen, P., Clapp, E., Clark, D., 1996. Refining estimates of ^{10}Be and ^{26}Al production rates. Radiocarbon 38, 149.

Bierman, P.R., Marsella, K.A., Patterson, C., Davis, P.T., Caffee, M., 1999. Mid-Pleistocene cosmogenic minimum-age limits for pre-Wisconsin glacial surfaces in southwestern Minnesota and southern Baffin Island: a multiple nuclide approach. Geomorphology 27, 25–39.

Briner, J.P., Miller, G.H., Davis, P.T., Bierman, P.R., Caffee, M., 2003. Last Glacial Maximum ice sheet dynamics in Arctic Canada inferred from young erratics perched on ancient tors. Quaternary Science Reviews 22 (5–7), 437–444.

Briner, J.P., Miller, G.H., Davis, P.T., Finkel, R., 2005. Cosmogenic exposure dating in Arctic glacial landscapes: implications for the glacial history of the Northeastern Baffin Island, Arctic Canada. Canadian Journal of Earth Sciences 42, 67–84.

Briner, J.P., Michelutti, N., Francis, D.M., Miller, G.H., Axford, Y., Wooller, M.J., Wolfe, A.P., 2006a. A multi-proxy lacustrine record of Holocene climate change on northeastern Baffin Island, Arctic Canada. Quaternary Research 65, 431–442.

Briner, J.P., Miller, G.H., Davis, P.T., Finkel, R.C., 2006b. Cosmogenic radionuclides from fiord landscapes support differential erosion by overriding ice sheets. Geological Society America Bulletin 118, 406–420.

Clarke, D.B., Upton, B.G.J., 1971. Tertiary Basalts of Baffin Island: field relations and tectonic setting. Canadian Journal Earth Sciences 8, 248–258.

Cuffey, K.M., Conway, H., Gades, A.M., Hallet, B., Lorrain, R., Severinghaus, J.P., Steig, E.J., Vaugh, B., White, J.W.C., 2001. Entrainment at cold glacier beds. Geology 28, 351–354.

Davis, P.T., Briner, J.P., Coulthard, R.D., Miller, G.H., Finkel, R.C., 2006. Preservation of Arctic landscapes overridden by cold-based ice sheets. Quaternary Research 65, 156–163.

Desilets, D., Zreda, M., 2003. Spatial and temporal distribution of secondary cosmic-ray nucleon intensities and applications to in-situ cosmogenic dating. Earth and Planetary Science Letters 206, 21–42.

Dunai, T.J., 2000. Scaling factors for the production rates of in-situ produced cosmogenic nuclides: a critical reevaluation. Earth and Planetary Science Letters 176, 159–171.

Dunai, T.J., 2001. Influence of secular variation of the geomagnetic field on production rates of in situ produced cosmogenic nuclides. Earth and Planetary Science Letters 193, 197–212.

Dyke, A.S., Andrews, J.T., Clark, P.U., England, J., Miller, G.H., Shaw, J., Veillette, J.J., 2001. Radiocarbon Dates Pertinent to Defining the Last Glacial Maximum for the Laurentide and Innuitian Ice Sheets. Geological Survey of Canada, Ottawa.

EPICA Community Members, 2004. Eight glacial cycles from an Antarctic ice core. Nature 429, 623–628.

Fabel, D., Fink, D., Fredin, O., Harbor, J., Land, M., Stroeven, A.P., 2006. Exposure ages from relict lateral moraines overridden by the Fennoscandian ice sheet. Quaternary Research 65, 136–146.

Feyling-Hanssen, R.W., 1976. The stratigraphy of the Quaternary Clyde Foreland formation, Baffin Island, illustrated by the distribution of benthic foraminifera. Boreas 5, 77–94.

Gosse, J., Klein, J., 1996. Production rate of in situ cosmogenic ^{10}Be in quartz at high altitude and mid latitude. Radiocarbon 38, 154–155.

Gosse, J.C., Phillips, F.M., 2001. Terrestrial in situ cosmogenic nuclides: theory and application. Quaternary Science Reviews 20, 1475–1560.

Heisinger, B., Lal, D., Jull, A.J.T., Kubik, P., Ivy-Ochs, S., Knie, K., Nolte, E., 2002. Production of selected cosmogenic radionuclides by muons: 2. Capture of negative muons. Earth and Planetary Science Letters 200, 357–369.

Hooke, R.L., Clausen, H.B., 1982. Wisconsin and Holocene δ^{18}O variations, Barnes Ice Cap, Canada. Geological Society of American Bulletin 93 (August), 784–789.

Hughes, T.J., 1998. Ice Sheets. Oxford University Press, New York, 343 pp.

Imbrie, J., Berger, A. and Shackleton, N.J., 1993. Role of orbital forcing: a two-million year perspective. In: Eddy, J.A. Oeschger H. (Eds.), Global Changes in the Perspective of the Past. Dahlem Workshop Reports, pp. 263–277.

Ives, J.D., 1966. Block fields, associated weathering forms on mountain tops and the Nunatak hypothesis. Geografiska Annaler 48A, 220–223.

Kaplan, M.R., Pfeffer, W.T., Sassolas, C., Miller, G.H., 1999. Numerical modeling of the Northeastern Laurentide Ice Sheet in the Baffin Island Region, Eastern Canadian Arctic: the role of a Cumberland Sound ice stream. Canadian Journal of Earth Sciences 36, 1315–1326.

Kleman, J., Stroeven, A.P., 1997. Preglacial surface remnants and Quaternary glacial regimes in northwestern Sweden. Geomorphology 19, 35–54.

Kohl, C.P., Nishiizumi, K., 1992. Chemical isolation of quartz for measurement of in situ-produced cosmogenic nuclides. Geochimica et Cosmochimica Acta 56, 3583–3587.

Kubik, P.W., Ivy-Ochs, S., 2004. A re-evaluation of the 0–10 ka ^{10}Be production rate for exposure dating obtained from the Köfels (Austria) landslide. Nuclear Instruments and Methods in Physics Research, B 223–224, 618–622.

Kubik, P.W., Ivy-Ochs, S., Masarik, J., Frank, M., Schlüchter, C., 1998. ^{10}Be and ^{26}Al production rates deduced from an instantaneous event within the dendro-calibration curve, the landslide of Köfels, Ötz Valley, Austria. Earth and Planetary Science Letters 161, 231–241.

Lal, D., 1991. Cosmic ray labeling of erosion surfaces: in situ nuclide production rates and erosion models. Earth and Planetary Science Letters 104, 424–439.

Lifton, N.A., Jull, A.J.T., Quade, J., 2001. A new extraction technique and production rate estimate for in situ cosmogenic ^{14}C in quartz. Geochimica et Cosmochimica Acta 65, 1953–1969.

Lifton, N.A., Bieber, J.W., Clem, J.M., Duldig, M.L., Evenson, P., Humble, J.E., Pyle, R., 2005. Addressing solar modulation and long-term uncertainties in scaling in situ cosmogenic nuclide production rates. Earth Planetary Science Letters 239, 140–161.

Locke, C.W., Locke, W.W.III., 1977. Little Ice Age snow-cover extent and paleoglaciation thresholds: north central Baffin Island, N.W.T., Canada. Arctic Alpine Research 9, 291–300.

Løken, O.H., 1965. Postglacial emergence at the south end of Inugsuin Fiord, Baffin Island, N.W.T. Geographical Bulletin 7, 243–258.

Løken, O.H., 1966. Baffin Island refugia older than 54,000 years. Science 153, 1378–1380.

Miller, G.H., 1973. Late Quaternary glacial and climatic history of northern Cumberland Peninsula, Baffin Island, N.W.T., Canada. Journal of Quaternary Research 3, 561–583.

Miller, G.H., Andrews, J.T., Short, S.K., 1977. The last interglacial–glacial cycle, Clyde foreland, Baffin Island, N.W.T.: stratigraphy, biostratigraphy, and chronology. Canadian Journal of Earth Sciences 14, 2824–2857.

Miller, G.H., Wolfe, A.P., Briner, J.P., Sauer, P.E., Nesje, A., 2005. Holocene glaciation and climate evolution of Baffin Island, Arctic Canada. Quaternary Science Reviews 24, 1703–1721.

National Oceanic and Atmospheric Administration, National Aeronautics and Space Administration, and United States Air Force, 1976. US Standard Atmosphere, Washington, DC, 227 pp.

Nishiizumi, K., 2004. Preparation of ^{26}Al AMS standards. Nuclear Instruments and Methods in Physics Research Section B: Beam Interactions with Materials and Atoms 223–224, 388–392.

Nishiizumi, K., Winterer, E.L., Kohl, C.P., Klein, J., Middleton, R., Lal, D., Arnold, J.R., 1989. Cosmic ray production rates of ^{10}Be and ^{26}Al in quartz from glacially polished rocks. Journal of Geophysical Research 94 (B12), 17,907–17,915.

Phillips, W.M., Halla, A.M., Mottrama, R., Fifield, L.K., Sugden, D.E., 2006. Cosmogenic ^{10}Be and ^{26}Al exposure ages of tors and erratics, Cairngorm Mountains, Scotland: timescales for the development of a classic landscape of selective linear glacial erosion. Geomorphology 73, 222–245.

Pigati, J.S., 2004. Experimental developments and application of carbon-14 and in situ cosmogenic nuclide dating techniques. Ph.D. Thesis, University of Arizona.

Smith, J.E., 1966. Sam Ford Fiord: a study in deglaciation. M.Sc. Thesis, McGill University, Montreal, 93 pp.

Stone, J.O., 2000. Air pressure and cosmogenic isotope production. Journal of Geophysical Research 105, 23,753–23,759.

Stroeven, A.P., Fabel, D., Hattestrand, C., Harbor, J., 2002. A relict landscape in the centre of Fennoscandian glaciation: cosmogenic radionuclide evidence of tors preserved through multiple glacial cycles. Geomorphology 44, 145–154.

Sugden, D.E., 1978. Glacial erosion by the Laurentide ice sheet. Journal of Glaciology 20, 367–391.